Coupling of k_z-dispersing π bands with surface localized states in graphite

Fumihiko Matsui (松井文彦)[1,2,*] and Shigemasa Suga (菅滋正)[3,4]

[1]*Institute for Molecular Science, Myodaiji, Okazaki 444-8585, Japan*
[2]*SOKENDAI (The Graduate University for Advanced Studies), Myodaiji, Okazaki 444-8585, Japan*
[3]*Forschungszentrum Jülich, Peter Grünberg Institut (PGI-6), Jülich 52425, Germany*
[4]*SANKEN, Osaka University, Ibaraki, Osaka 567-0047, Japan*

(Received 1 April 2022; accepted 6 June 2022; published 21 June 2022)

The graphite k_z dispersion from the region with a size of several micrometers was measured via photoelectron momentum microscopy. The π-band dispersion over an entire Brillouin zone was investigated. We found that the degeneracy of the π bands was eliminated in the ALH reciprocal lattice plane and their symmetries were reduced from C_{6v} to C_{3v}. We attributed this phenomenon to the coupling of the graphite surface π band of a single-domain threefold structure with the sixfold bulk k_z dispersion which has been neglected to date. We used this symmetry breaking to image the monoatomic step of the graphite surface. Further, the precision of determining k_z dispersion and the effect of surface resonance are discussed.

DOI: 10.1103/PhysRevB.105.235126

I. INTRODUCTION

The electronic structures of solids and surfaces can be revealed by angle-resolved photoelectron spectroscopy (ARPES) based on the laws of energy and momentum conservation during photoemission. Energy tunable synchrotron radiation assessing bulk k_z dispersion information has been applied to many materials [1–18]. Soft x-ray excitation has the advantage of a large photoelectron emission cross-section of valence-band electrons. However, the information from detected photoelectrons is limited within the surface region due to the photoelectron's shorter mean-free-path length, λ_z, than that of bulk-sensitive measurement by hard x-ray excitation [19]. Crossover from a two- to three-dimensional electronic structure has been discussed for several layered materials [8–13]. Disentangling surface resonance states from the bulk electronic structure of topological materials [14,15] and black phosphorus [16,17] using ARPES, for instance, is a contemporary issue.

The surface electronic state of graphite was investigated via scanning tunneling microscopy [20–22] and core-level photoelectron spectroscopy [23–25]. In graphite k_z dispersion research, however, surface state contribution has not yet been discussed to the best of our knowledge [1–7]. We revisited the graphite k_z dispersion via μm-area selective ARPES [26–28]. In this study, we report the observation of threefold symmetric surface states coupled with bulk k_z dispersed π bands. The finding highlights the relevance of considering surface effects in bulk electronic state measurements. The question we address is as follows: *How accurate can we measure the k_z dispersion?*

II. EXPERIMENTAL DETAILS

Selected graphite hexagonal crystal flakes were mounted on a sample holder, cleaved in air, and degassed at 500 °C under ultrahigh vacuum conditions [7,29–31]. Valence-band dispersion was measured using a photoelectron momentum microscope (PMM) [26–28] at the linear polarization soft x-ray beamline BL6U of the UVSOR Synchrotron Facility, Japan [32]. The sample temperature was kept at 15 K during the measurement.

One of the ΓK directions was aligned horizontally toward the a/k_a axis. C-C bonds (ΓM directions) perpendicular to the a/k_a axis were aligned vertically along the b/k_b axis. The surface normal direction was aligned to the axis of the analyzer (z). The axis of the incident light was positioned at $\theta_{\rm in} = 68^\circ$ off from the z axis. The electric vector of the incident light was within the a-z plane. Photon energy was varied from 52.0 to 120.0 eV to observe valence-band k_z dispersion in two Brillouin zones (BZs). Using the photoemission electron microscope lens of the PMM, the magnified sample image by 400 times was projected onto a hemispherical analyzer entrance aperture of 0.2 mm × 0.8 mm. Photoelectrons within a few μm in diameter on the sample surface were selected for momentum-resolved photoelectron momentum distribution (PMD) analysis with an acceptance diameter of 4 Å^{-1}. This acceptance diameter is independent of the kinetic energy of the photoelectrons in the PMM measurement. The work function and the pass energy of the PMM were 4.523 and 10.0 eV, respectively.

III. RESULTS AND DISCUSSION

Figures 1(a)–1(i) show a series of graphite valence-band PMD patterns with binding energies (BEs) of 2.5 and 3.0 eV excited by various photon energies. The hexagonal BZ of graphite is indicated in Figs. 1(a) and 1(j). As shown in

*matui@ims.ac.jp

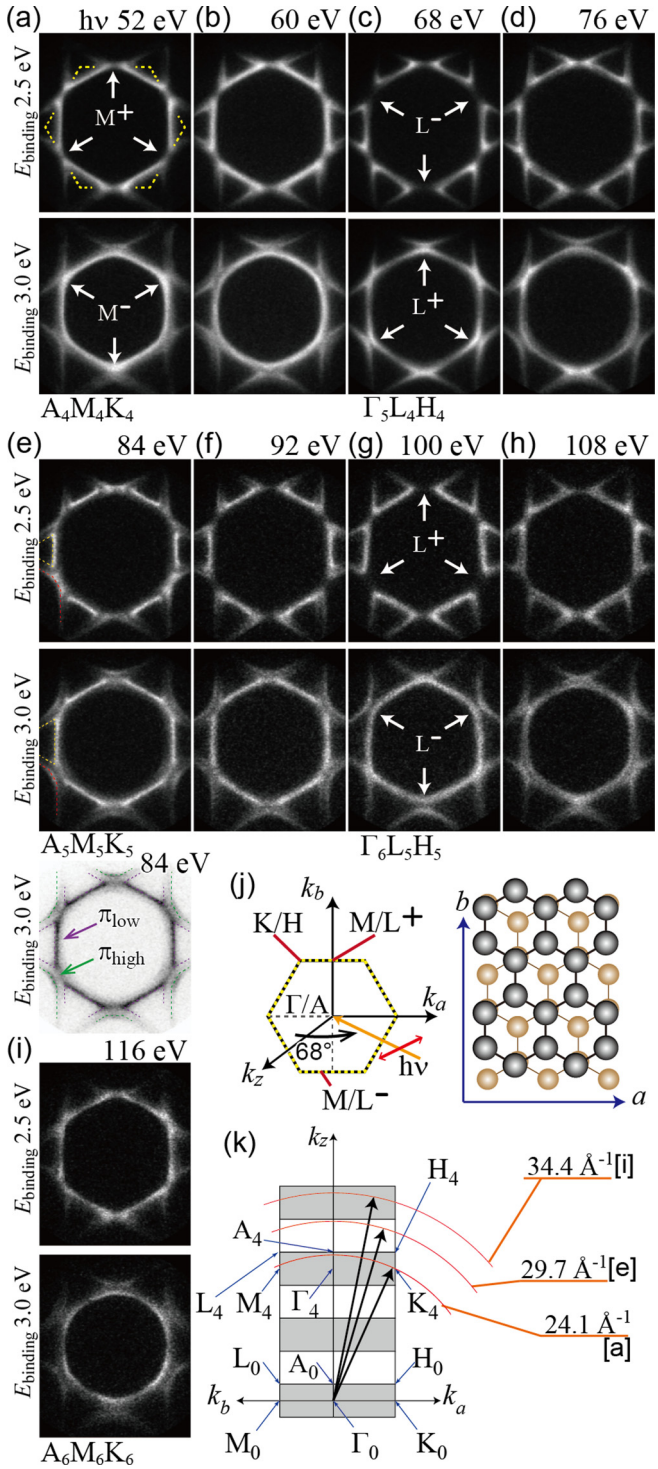

FIG. 1. (a)–(i) The graphite valence-band PMD patterns with BEs of 2.5 and 3.0 eV excited by various photon energies. Hexagonal BZ is indicated in (a) and (j). BZs stacked in the k_z direction and photoelectron wavevectors corresponding to (a), (e), and (i) are shown in (k).

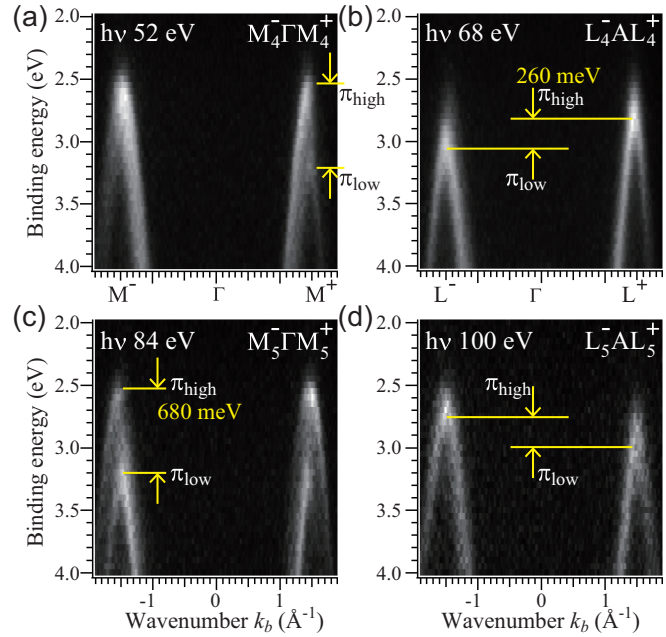

FIG. 2. The graphite π band dispersions along the $M^-\Gamma M^+$ and L^-AL^+ directions. Two π bands are observed in the $M^-\Gamma M^+$ direction, (a) and (c), whereas they degenerate in the L^-AL^+ direction, (b) and (d).

Fig. 1(k), photoelectrons from the vicinity of the M and K points are detected by the excitation with photon energies of (a) 52.0, (e) 84.0, and (i) 116.0 eV, whereas photoelectrons from the vicinity of the L and H points are detected by the excitation with photon energies of (c) 68.0 and (g) 100.0 eV. An inner potential value of 17.17 eV was used to estimate the wavenumber [7]. The M points on the $+k_b$ and $-k_b$ sides, and their C_{3v} symmetric equivalent points are denoted as M^+ and M^-, respectively [Fig. 1(a)]. The L points on the $+k_b$ and $-k_b$ sides and their C_{3v} symmetric equivalent points are denoted as L^+ and L^-, respectively [Figs. 1(c) and 1(g)].

Sixfold symmetric cross-sections of the π band on the $A_4M_4K_4$ and $A_6M_6K_6$ spherical surfaces were obtained for 52-eV [Fig. 1(a)] and 116-eV [Fig. 1(i)] excitations, respectively. The cross-sections of the π band at the $A_5M_5K_5$ spherical surface were obtained for 84-eV excitation [Fig. 1(e)]. Note that in the latter case (e), the degenerated π band was split into two branches, namely, into the π_{low} and π_{high} bands, and their separate cross-sections were observed [bottom figure in Fig. 1(e)].

The two bands, π_{high} and π_{low}, are recognized at the M^+ and M^- points [Figs. 2(a) and 2(c)], whereas only one band is observed at the L^+ and L^- points [Figs. 2(b) and 2(d)]. Hereinafter, instead of the exact k_z value, the notation of Γ or A at the same k_z as M/K or L/H is used, because there are no bands along the Γ/A axis in this BE range. The π_{high} and π_{low} bands at the M point were separated by 680 meV. The π_{high} and π_{low} bands were observed in the first and second BZs, respectively, for 52-eV excitation [Fig. 2(a)] and visa versa for the 84-eV excitation [Fig. 2(c)]. The photoelectron intensity outside the first BZ is darker than the inside intensity. These intensity modulations are due to the photoelectron interference from four different carbon atoms in the unit cell, namely, the photoelectron structure factor effect [7,33–36].

As shown in Figs. 2(b) and 2(d), the π-band saddle energy at the L^+ and L^- points differed by 260 meV, yielding the symmetry breaking of the PMD patterns. The cross-section of the π band with 2.5-eV BE is triangular and surrounds the K/H point regardless of any excitation photon energy [Figs. 1(a)–1(i)]. With an increase in BE up to 3.0 eV, the π band expands toward the M/L points, forming a central hexagonal round shape. In this study, we found that for 68- and 100-eV excitations, the symmetry is reduced from C_{6v} to C_{3v}. The above-mentioned π triangle features around the K/H point at 2.5-eV BE show gaps at the L^+ and L^- points for 68- and 100-eV excitations, respectively [Figs. 1(c) and 1(g)]. Further, the hexagonal round shape in the first BZ at 3.0-eV BE touched with the second BZ band at the L^+ and L^- points for 68- and 100-eV excitations, respectively.

The axis of the detector and the incident photon direction form a mirror-symmetry plane *a*-*z*, whereas the crystal *surface* mirror plane is aligned to the *b*-*z* plane. Note that graphite crystals with an *ABAB*$\cdots$-type stacking structure are sixfold symmetric around the *z* axis, whereas a surface with one type of termination is threefold symmetric. Therefore the inversion of symmetry at the L_4^+ and the L_5^- points [Figs. 1(c) and 1(g)] is due to the *surface* structure of the sample. The microscope function of the PMM has a merit of the detection area sufficiently small to select only one type of graphite termination structure on the cleavage plane.

Figure 3(a) shows the graphite π band k_z dispersion along the M/L axis. Intensity profiles from the six M/L axes were added to each data point. The sinusoidal curves (dotted and dashed lines) in Fig. 3(a) show the π band k_z dispersion. Their amplitudes were fixed at 680 meV, which was the energy splitting value at the M point in Figs. 2(a) and 2(c). The edges of the curves were fixed at the M points. The center of the sinusoidal curves was located at 2.90-eV BE. The PMD patterns in Fig. 1 and the band dispersions in Fig. 2 show that the π-band k_z dispersions along the $M^{\pm}/L^{\pm}$ axes are not equivalent. Therefore the graphite π-band k_z dispersions along the M^+/L^+ and M^-/L^- axes must be plotted individually [Figs. 3(b) and 3(c), respectively]. The sinusoidal curves with the half wavelength of Fig. 3(a) are used in Figs. 3(b) and 3(c). The gap between the two curves was set to 260 meV.

The intensity difference between the graphite π-band k_z dispersions along the M^+/L^+ and M^-/L^- is shown in Fig. 3(d). The red or blue part corresponds to where the intensity along the M^+/L^+ axis is stronger or weaker than that along the M^-/L^- axis. Notably, the maximum and minimum intensity differences appear at points shifted by 0.3 $Å^{-1}$ below the M and L points, respectively, on the M/L axis but not at the high symmetric reciprocal lattice points.

Figures 4(a)–4(d) show the graphite π-band atomic-orbital configurations at the M and L points. There are two bands, π_{low} [Figs. 4(a) and 4(b)] and π_{high} [Figs. 4(c) and 4(d)], with a bonding and an antibonding interlayer atomic-orbital configuration within a unit cell. The *bulk* π_{low} and π_{high} bands have different BEs at the M point as seen in Figs. 2(a) and 2(c) (all bonding or antibonding), whereas they degenerate at the L point (bonding and antibonding alternatively). The bonding interaction is removed for Figs. 4(a) and 4(d), whereas antibonding interaction is removed for Figs. 4(b) and 4(c) by cleavage. Owing to the broken symmetry of the surface,

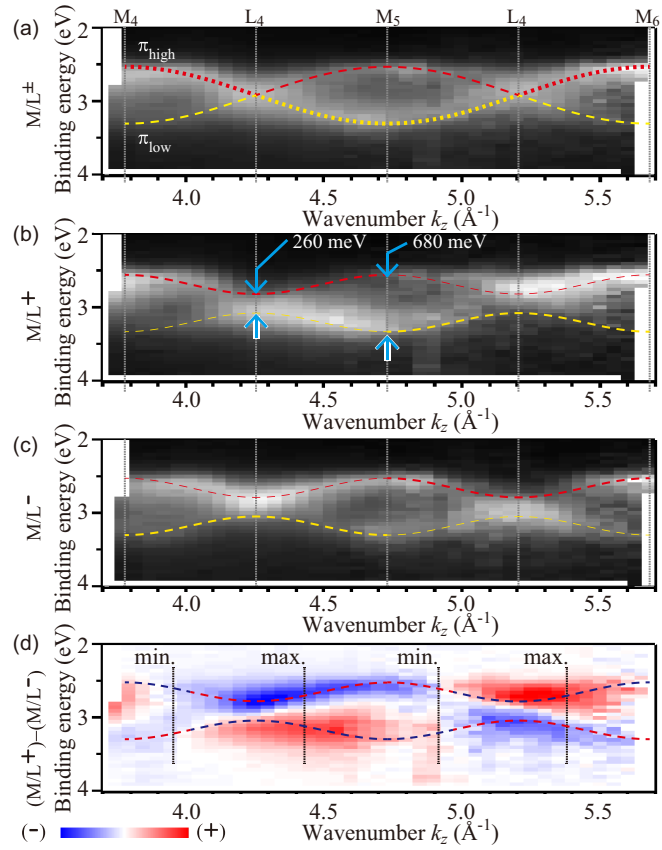

FIG. 3. The graphite π band k_z dispersion along the (a) M/L axis. Owing to the broken symmetry on the surface, the degenerated π band at the A point is split in two. The graphite π band k_z dispersions along (b) the M^+/L^+ and (c) M^-/L^- axes and (d) their difference.

the degenerated π bands at the L points are split into two branches. Then we conclude that the degeneracy at the L points is because of the coupling of the surface state with the bulk k_z dispersed π band by this cleavage. Because the symmetry breaking exists only in the topmost two graphite layers, the energy splitting at the L points is attributed to the initial surface electronic structure. The hybrid of surface and bulk electronic states has been observed in monolayer Ni films on Cu (001) substrates and has been deeply discussed based on the *hetero*-interaction of Ni 3d and Cu sp bands [37–39]. The current case of the *homo*-interaction between the graphite surface and the bulk π bands was finally detected using the symmetry breaking on the outermost surface.

The k_z symmetry breaking of the photoelectron intensity along the M/L axis in Fig. 3(d) was not symmetric with respect to the M point, unlike the photoelectron structure factor effect which is solely determined by the atomic-orbital configuration of the initial state [7]. The interference between photoelectrons from the surface bilayer atomic orbitals arranged locally in threefold symmetry results in intensity modification [30,40]. Simplified models of constructive and destructive interferences causing the threefold symmetry are shown in Figs. 4(e) and 4(f), respectively. This interference depends on the kinetic energy of the photoelectrons and

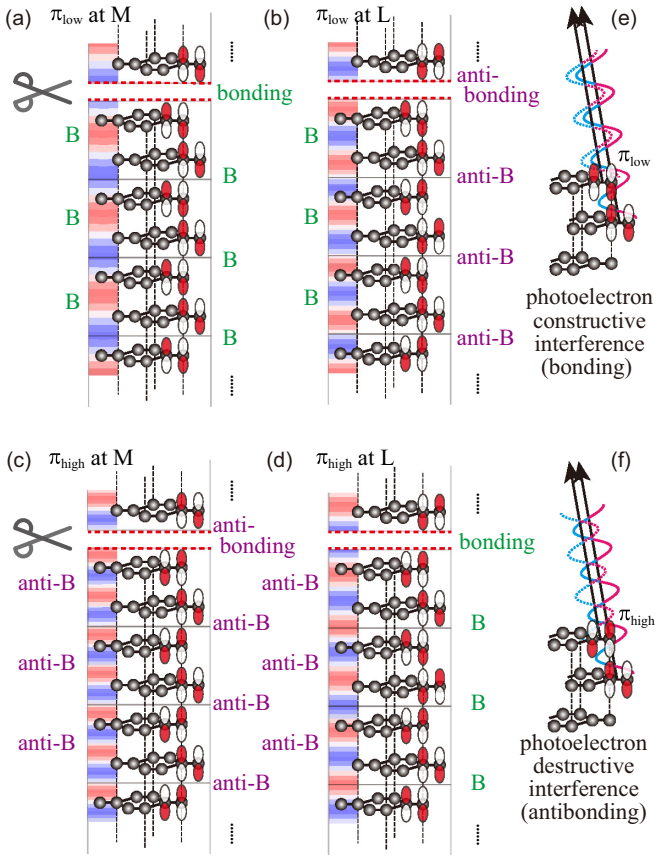

FIG. 4. The graphite π_{low} band atomic-orbital configurations at the (a) M and (b) L points and the π_{high} band atomic-orbital configurations at the (c) M and (d) L points. Bonding interaction is removed for (a) and (d), whereas antibonding interaction is removed for (b) and (c) by cleavage. Degeneracy in the ALH symmetry plane is eliminated by this cleavage. "B" denotes "bonding." Photoelectron interference effect from the surface bilayer atomic orbitals; (e) constructive and (f) destructive cases.

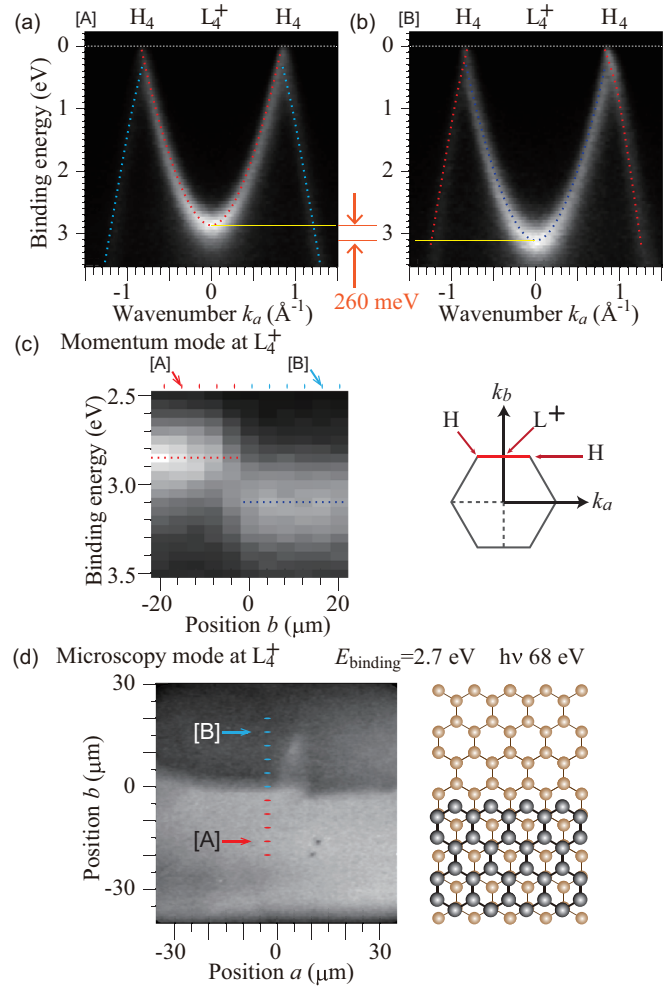

FIG. 5. (a) and (b) The π-band dispersion along the $H_4L_4^+H_4$ direction at two positions [A] and [B], respectively. Photon energy was 68 eV. (c) Photoelectron spectra of the L_4^+ point measured at the various positions indicated by red and blue dots in (d). (d) Microscopic image around the positions [A] and [B]. Photoelectrons from the L_4^+ point and 2.7-eV BE were selected. The boundary is attributed to a zigzag-type monoatomic step of the graphite.

explains the k_z symmetry breaking with respect to the M point. Further theoretical study based on a multiple-scattering calculation for the valence photoelectron emission is desired to elucidate the k_z intensity dependence.

The surface terminations, $ABAB\cdots$ and $BABA\cdots$, can be specified by using the threefold symmetry of the PMD at the L point with 68-eV excitation. Figures 5(a) and 5(b) show the π-band dispersion along the $H_4L_4^+H_4$ direction at two positions, [A] and [B], on the surface shown in Fig. 5(d). Notably, the BEs of the parabolic dispersion bottoms at the two positions differ by 260 meV. As shown in Fig. 5(c), the bottom energy changed stepwise as the position was scanned. Figure 5(d) is the microscopy-mode image around the positions [A] and [B]. Intensity of photoelectrons from the L_4^+ point with the 2.7-eV BE was selected and plotted. Red and blue dots in Fig. 5(d) indicate the areas where the momentum-mode photoelectron spectra shown in Fig. 5(c) were measured. The boundary between the different contrast regions in Fig. 5(d) is aligned along the HLH direction. Thus the boundary is attributed to the zigzag-type graphite monoatomic step [22].

The current observations provide us a hint to the question presented earlier: *How accurate can we measure the k_z dispersion?* The k_z resolution is often defined by the inverse of the photoelectron inelastic mean-free path, λ_z, as $\Delta k_z > \lambda_z^{-1}$ [41,42]. In this case, λ_z is less than 1 nm [30], which corresponds to the thickness of several atomic layers. However, the observed bulk dispersion differs from the discrete electronic states of several layers of graphene [4], meaning that the measurement is also sensitive to the bulk electronic states from much deeper than λ_z. Thus the precision of the k_z dispersion periodicity is determined by almost one order of magnitude better than the inverse of the λ_z. Moreover, the k_z dispersion bandwidth is affected by the coupling with the surface electronic state, as shown in this study. The accuracy and resolution of k_z dispersion bandwidth determination are limited by λ_z attenuation [43], especially when the surface resonance state couples with the bulk k_z-dispersed band.

IV. CONCLUSION

In conclusion, the graphite k_z dispersion from several μm regions was measured using the PMM. The π-band dispersion across two complete BZs was investigated. We found that in the ALH plane, the degeneracy of the π bands was eliminated, and their symmetries were reduced from C_{6v} to C_{3v}. This phenomenon is attributed to the coupling of the graphite surface state of a single-domain threefold structure with the sixfold bulk k_z dispersed π band. We used this symmetry breaking to image the monoatomic step of the graphite surface. Note that surface resonance must be considered when determining the k_z dispersion, although the existing photoemission measurements neglected such an effect, with few exceptions [36,44]. So far valence-band mapping measurements from large areas have yielded an average signal acquisition from twin domains. In this study, we have succeeded in characterizing the effect of such a coupling in a surface geometry with broken symmetry using μm-area-selective valence-band mapping and momentum-resolved photoelectron microscopy [28].

ACKNOWLEDGMENTS

We acknowledge Dr. Christian Tusche and Prof. Claus M. Schneider [Forschungszentrum Jülich (FZJ), PGI-6] for their valuable advice through the framework of international collaboration between FZJ and the Institute for Molecular Science (IMS). We are deeply grateful to Dr. Marcus Breusing, Dr. Marko Wietstruk, Dr. Mirko Weidner (SPECS), Dr. Dai Yamaguchi (Tokyo Instruments Inc.), Prof. Satoshi Kera (IMS), and the staffs of UVSOR synchrotron facility for their contribution to the construction of the PMM experimental station. We acknowledge the financial support by JSPS, Fostering Joint International Research (B), No. 19KK0137.

[1] D. Marchand, C. Frétigny, M. Laguës, F. Batallan, Ch. Simon, I. Rosenman, and R. Pinchaux, Phys. Rev. B **30**, 4788 (1984).
[2] A. R. Law, M. T. Johnson, and H. P. Hughes, Phys. Rev. B **34**, 4289 (1986).
[3] T. Kihlgren, T. Balasubramanian, L. Walldén, and R. Yakimova, Phys. Rev. B **66**, 235422 (2002).
[4] T. Ohta, A. Bostwick, J. L. McChesney, T. Seyller, K. Horn, and E. Rotenberg, Phys. Rev. Lett. **98**, 206802 (2007).
[5] A. Grüneis, T. Pichler, H. Shiozawa, C. Attaccalite, L. Wirtz, S. L. Molodtsov, R. Follath, R. Weber, and A. Rubio, Phys. Status Solidi B **244**, 4129 (2007).
[6] A. Grüneis, C. Attaccalite, T. Pichler, V. Zabolotnyy, H. Shiozawa, S. L. Molodtsov, D. Inosov, A. Koitzsch, M. Knupfer, J. Schiessling, R. Follath, R. Weber, P. Rudolf, L. Wirtz, and A. Rubio, Phys. Rev. Lett. **100**, 037601 (2008).
[7] F. Matsui, H. Nishikawa, H. Daimon, M. Muntwiler, M. Takizawa, H. Namba, and T. Greber, Phys. Rev. B **97**, 045430 (2018).
[8] M. C. Schabel, C.-H. Park, A. Matsuura, Z.-X. Shen, D. A. Bonn, X. Liang, and W. N. Hardy, Phys. Rev. B **57**, 6090 (1998).
[9] A. Bansil, M. Lindroos, S. Sahrakorpi, and R. S. Markiewicz, Phys. Rev. B **71**, 012503 (2005).
[10] M. Lindroos, S. Sahrakorpi, V. Arpiainen, R. S. Markiewicz, and A. Bansil, J. Phys. Chem. Solids **67**, 244 (2006).
[11] S. Thirupathaiah, E. D. L. Rienks, H. S. Jeevan, R. Ovsyannikov, E. Slooten, J. Kaas, E. van Heumen, S. de Jong, H. A. Dürr, K. Siemensmeyer, R. Follath, P. Gegenwart, M. S. Golden, and J. Fink, Phys. Rev. B **84**, 014531 (2011).
[12] Y. Wu, Y. Lee, T. Kong, D. Mou, R. Jiang, L. Huang, S. L. Bud'ko, P. C. Canfield, and A. Kaminski, Phys. Rev. B **96**, 035134 (2017).
[13] L. Miao, S. Liu, Y. Xu, E. C. Kotta, C.-J. Kang, S. Ran, J. Paglione, G. Kotliar, N. P. Butch, J. D. Denlinger, and L. A. Wray, Phys. Rev. Lett. **124**, 076401 (2020).
[14] D. Hsieh, L. Wray, Y. Xia, J. H. Dil, F. Meier, L. Patthey, J. Osterwalder, G. Bihlmayer, Y. S. Hor, R. J. Cava, and M. Z. Hasan, New J. Phys. **12**, 125001 (2010).
[15] J. Sánchez-Barriga, M. G. Vergniory, D. Evtushinsky, I. Aguilera, A. Varykhalov, S. Blügel, and O. Rader, Phys. Rev. B **94**, 161401(R) (2016).
[16] C. Q. Han, M. Y. Yao, X. X. Bai, L. Miao, F. Zhu, D. D. Guan, S. Wang, C. L. Gao, C. Liu, D. Qian, Y. Liu, and J.-F. Jia, Phys. Rev. B **90**, 085101 (2014).
[17] E. Golias, M. Krivenkov, and J. Sánchez-Barriga, Phys. Rev. B **93**, 075207 (2016).
[18] H. J. Elmers, J. Regel, T. Mashoff, J. Braun, S. Babenkov, S. Chernov, O. Fedchenko, K. Medjanik, D. Vasilyev, J. Minar, H. Ebert, and G. Schönhense, Phys. Rev. Research **2**, 013296 (2020).
[19] M. Yano, A. Sekiyama, H. Fujiwara, Y. Amano, S. Imada, T. Muro, M. Yabashi, K. Tamasaku, A. Higashiya, T. Ishikawa, Y. Onuki, and S. Suga, Phys. Rev. B **77**, 035118 (2008).
[20] D. Tománek, S. G. Louie, H. J. Mamin, D. W. Abraham, R. E. Thomson, E. Ganz, and J. Clarke, Phys. Rev. B **35**, 7790 (1987).
[21] Y. Sugawara, T. Ishizaka, S. Morita, S. Imai, and N. Mikoshiba, Jpn. J. Appl. Phys. **29**, L157 (1990).
[22] Y. Kobayashi, K. I. Fukui, T. Enoki, K. Kusakabe, and Y. Kaburagi, Phys. Rev. B **71**, 193406 (2005).
[23] T. Balasubramanian, J. N. Andersen, and L. Wallden, Phys. Rev. B **64**, 205420 (2001).
[24] R. A. P. Smith, C. W. Armstrong, G. C. Smith, and P. Weightman, Phys. Rev. B **66**, 245409 (2002).
[25] A. Šimůnek and J. Vackář, Phys. Rev. B **69**, 073403 (2004).
[26] F. Matsui, S. Makita, H. Matsuda, T. Yano, E. Nakamura, K. Tanaka, S. Suga, and S. Kera, Jpn. J. Appl. Phys. **59**, 067001 (2020).
[27] S. Makita, H. Matsuda, Y. Okano, T. Yano, E. Nakamura, Y. Hasegawa, S. Kera, S. Suga, and F. Matsui, e-J. Surf. Sci. Nanotechnol. **19**, 42 (2021).
[28] F. Matsui, Y. Okano, H. Matsuda, T. Yano, E. Nakamura, S. Kera, and S. Suga, J. Phys. Soc. Jpn. (2022) submitted.
[29] F. Matsui, S. Makita, H. Matsuda, E. Nakamura, Y. Okano, T. Yano, S. Kera, and S. Suga, J. Phys. Soc. Jpn. **90**, 124710 (2021).
[30] F. Matsui, T. Matsushita, and H. Daimon, J. Phys. Soc. Jpn. **81**, 114604 (2012).

[31] F. Matsui, S. Makita, H. Matsuda, T. Ohigashi, H. Yamane, and N. Kosugi, J. Phys. Soc. Jpn. **88**, 114704 (2019).
[32] H. Yamane, F. Matsui, T. Ueba, T. Horigome, S. Makita, K. Tanaka, S. Kera, and N. Kosugi, Rev. Sci. Instrum. **90**, 093102 (2019).
[33] H. Daimon, S. Imada, H. Nishimoto, and S. Suga, J. Electron. Spectrosc. Relat. Phenom. **76**, 487 (1995).
[34] H. Nishimoto, T. Nakatani, T. Matsushita, S. Imada, H. Daimon, and S. Suga, J. Phys.: Condens. Matter **8**, 2715 (1996).
[35] E. L. Shirley, L. J. Terminello, A. Santoni, and F. J. Himpsel, Phys. Rev. B **51**, 13614 (1995).
[36] F. Matsui, T. Matsushita, and H. Daimon, J. Electron. Spectrosc. Relat. Phenom. **195**, 347 (2014).
[37] G. J. Mankey, K. Subramanian, R. L. Stockbauer, and R. L. Kurtz, Phys. Rev. Lett. **78**, 1146 (1997).
[38] O. Rader, H. Wolf, W. Gudat, A. Tadich, L. Broekman, E. Huwald, R. C. G. Leckey, J. D. Riley, A. M. Shikin, F. Matsui, H. Miyata, and H. Daimon, Phys. Rev. B **79**, 245104 (2009).
[39] M. Hoesch, V. N. Petrov, M. Muntwiler, M. Hengsberger, J. L. Checa, T. Greber, and J. Osterwalder, Phys. Rev. B **79**, 155404 (2009).
[40] F. Matsui, R. Ishii, H. Matsuda, M. Morita, S. Kitagawa, T. Matsushita, S. Koh, and H. Daimon, Jpn. J. Appl. Phys. **52**, 110110 (2013).
[41] F. J. Himpsel, Adv. Phys. **32**, 1 (1983).
[42] M. Horio, K. Hauser, Y. Sassa, Z. Mingazheva, D. Sutter, K. Kramer, A. Cook, E. Nocerino, O. K. Forslund, O. Tjernberg, M. Kobayashi, A. Chikina, N. B. M. Schroter, J. A. Krieger, T. Schmitt, V. N. Strocov, S. Pyon, T. Takayama, H. Takagi, O. J. Lipscombe *et al.*, Phys. Rev. Lett. **121**, 077004 (2018).
[43] V. N. Strocov, J. Electron. Spectrosc. Relat. Phenom. **130**, 65 (2003).
[44] K. Sugawara, T. Sato, S. Souma, T. Takahashi, and H. Suematsu, Phys. Rev. B **73**, 045124 (2006).